

# Stark effect modeling in the detailed opacity code SCO-RCG

Jean-Christophe Pain<sup>a,1</sup>, Franck Gilleron<sup>a</sup> and Dominique Gilles<sup>b</sup>

<sup>a</sup> CEA, DAM, DIF, F-91297 Arpajon, France

<sup>b</sup> CEA, DSM, IRFU, F-91191 Gif-sur-Yvette, France

## Abstract

The broadening of lines by Stark effect is an important tool for inferring electron density and temperature in plasmas. Stark-effect calculations often rely on atomic data (transition rates, energy levels,...) not always exhaustive and/or valid for isolated atoms. We present a recent development in the detailed opacity code SCO-RCG for K-shell spectroscopy (hydrogen- and helium-like ions). This approach is adapted from the work of Gilles and Peyrusse. Neglecting non-diagonal terms in dipolar and collision operators, the line profile is expressed as a sum of Voigt functions associated to the Stark components. The formalism relies on the use of parabolic coordinates within SO(4) symmetry. The relativistic fine-structure of Lyman lines is included by diagonalizing the hamiltonian matrix associated to quantum states having the same principal quantum number  $n$ . The resulting code enables one to investigate plasma environment effects, the impact of the microfield distribution, the decoupling between electron and ion temperatures and the role of satellite lines (such as Li-like  $1snl'n'l' - 1s^2nl$ , Be-like, etc.). Comparisons with simpler and widely-used semi-empirical models are presented.

## 1 Introduction and outline of the method

In hot dense plasmas encountered for instance in inertial confinement fusion (ICF), the line broadening resulting from Stark effect can be used as a diagnostics of electronic temperature  $T_e$ , density  $n_e$  and ionic temperature  $T_i$ . This represents a challenging task, since from astrophysical dilute plasmas to ultra-dense nuclear fuel in ICF, the density varies by twenty orders of magnitude. The capability of the detailed opacity code SCO-RCG [1, 2] was recently extended to K-shell spectroscopy (hydrogen- and helium-like ions), following an approach proposed by Gilles and Peyrusse [3]. Ions and electrons are treated respectively in the quasi-static and impact approximations and the line profile reads

$$\phi(\nu) \propto \frac{1}{\pi} \int \text{Re} \left[ \text{Tr} \{ \hat{d} \cdot \hat{X}^{-1} \} \right] W(F) dF, \quad (1)$$

where  $\hat{X} = 2i\pi(\nu + \nu_1) - i\hat{H}(F)/\hbar - \hat{\Lambda}_c$ ,  $\nu_1$  being the frequency of the lower state and  $\hat{H}(F) = \hat{H}_0 - \hat{d} \cdot F$  the hamiltonian of the ion in the presence of an electric field  $F$  following the normalized distribution  $W(F)$ .  $\hat{H}_0$  is the hamiltonian without electric field while  $\hat{d}$  and  $\hat{\Lambda}_c$  represent respectively the dipole and collision operators. The trace (Tr) runs over the various states of the upper level. If  $\Delta\nu_D$  is the Doppler width and  $w_k$  the weight of the  $k^{\text{th}}$  Stark component, neglecting non-diagonal terms in dipolar and collision operators, the line profile can be written as a sum of Voigt ( $V$ ) functions (parametrized as in Ref. [4]):

---

<sup>1</sup>jean-christophe.pain@cea.fr (corresponding author)

$$\phi(\nu) = \frac{1}{\sqrt{\pi}} \frac{1}{\Delta\nu_D} \int_0^\infty W(F) dF \left[ \sum_k w_k(F) V(x_k, y_k) \right] ; \quad x_k = \frac{\nu - \nu_0 - c_k(F)}{\Delta\nu_D} ; \quad y_k = \frac{\langle k | \hat{\Lambda}_c | k \rangle}{2\pi\Delta\nu_D}, \quad (2)$$

where  $\nu_0$  is the frequency of the line without external field and

$$c_k(F) = \langle k | -\hat{d}\cdot F | k \rangle ; \quad \hat{\Lambda}_c = \frac{4\pi}{3} n_e \left( \frac{e}{\hbar} \right)^2 \hat{d}\cdot\hat{d} \left( \frac{2m}{\pi k_B T_e} \right)^{1/2} \ln \left( \frac{\lambda_{DH} Z}{n^2 a_0} \right), \quad (3)$$

$\lambda_{DH}$  being the Debye-Hückel length.

## 2 Hydrogen-like ions

Stark effect for hydrogenic ions can be calculated in parabolic coordinates using the basis states  $|nqm_\ell\rangle$ , where  $q = n_1 - n_2$ ,  $n_1$  and  $n_2$  being the so-called parabolic quantum numbers, related by  $n_1 + n_2 + |m_\ell| + 1 = n$ ,  $-\ell \leq m_\ell \leq \ell$  being the magnetic orbital quantum number. The perturbation  $\hat{d}$  is diagonal in this basis and a  $2^{nd}$ -order development gives

$$\langle nqm_\ell | -\hat{d}\cdot F | nqm_\ell \rangle = \frac{3ea_0}{2} \frac{nqF}{Z} - \frac{1}{16} \frac{e^2 a_0^2}{(2Ry)} \left( \frac{n}{Z} \right)^4 (17n^2 - 3q^2 - 9m_\ell^2 + 19) F^2. \quad (4)$$

However, the fine-structure hamiltonian  $\hat{H}_0$  is diagonal in the subset of states  $|nlsjm_j\rangle$ . In order to diagonalize the total hamiltonian  $\hat{H}$  in such a basis, the Stark matrix element is

$$\begin{aligned} \langle nlsjm_j | -\hat{d}\cdot F | n\ell'sj'm_j \rangle &= \sum_{m_s=-1/2}^{1/2} \sum_{q=-(n-1-|m_\ell|)}^{n-1-|m_\ell|, 2} (-1)^{\ell+\ell'-1+3m_j-m_s-q-n} [\ell, \ell', j, j']^{1/2} \\ &\times \begin{pmatrix} \ell & s & j \\ m_\ell & m_s & -m_j \end{pmatrix} \begin{pmatrix} \ell' & s & j' \\ m_\ell & m_s & -m_j \end{pmatrix} \\ &\times \begin{pmatrix} \frac{n-1}{2} & \frac{n-1}{2} & \ell \\ \frac{m_\ell-q}{2} & \frac{m_\ell+q}{2} & -m_\ell \end{pmatrix} \begin{pmatrix} \frac{n-1}{2} & \frac{n-1}{2} & \ell' \\ \frac{m_\ell-q}{2} & \frac{m_\ell+q}{2} & -m_\ell \end{pmatrix} \\ &\times \langle nqm_\ell | -\hat{d}\cdot F | nqm_\ell \rangle, \end{aligned} \quad (5)$$

with  $s = 1/2$ ,  $m_\ell + m_s = m_j$  and  $[x] = 2x + 1$ . Fig. 1 displays a comparison between our previous semi-empirical modeling (Refs. [5, 6]) and the present work in the case of Ar XVIII Ly $_\alpha$  line. Fig. 2 shows Mg XII Ly $_\beta$  profile in three different conditions.

## 3 Helium-like ions

We consider the transitions  $1sn\ell^1P-1s^2$ ,  $n \geq 2$ . For  $n \geq 5$ , the perturbation due to field  $F$  is much larger than the separation between terms, the levels are quasi-hydrogenic and He lines are modeled as Ly-like lines (with  $Z \rightarrow Z - 1$ ). For  $n < 5$ , singlet-triplet mixing is neglected and two-electron wavefunctions  $\Psi(1, 2)$  of singlet states are built as [9]:

$$\Psi(1, 2) = \frac{1}{\sqrt{2}} [\psi_{100}^Z(1)\psi_{n\ell m_\ell}^{Z-1}(2) \pm \psi_{n\ell m_\ell}^{Z-1}(1)\psi_{100}^Z(2)] \times \chi_{a(+),s(-)} \quad (6)$$

where  $\psi_{100}^Z$  is the wavefunction of the fundamental state of an hydrogenic ion of charge  $Z$  and  $\psi_{n\ell m_\ell}^{Z-1}$  the wavefunction of the excited state  $n\ell m_\ell$  of an hydrogenic ion of charge  $Z - 1$ .  $\chi_{a,s}$  are antisymmetric (resp. symmetric) spin functions. Such an approximation is valid for highly charged ions when the electron-nucleus interaction overcomes the Coulomb electron-electron repulsion. The hamiltonian  $\hat{H}_0 - e(z_1 + z_2)F$

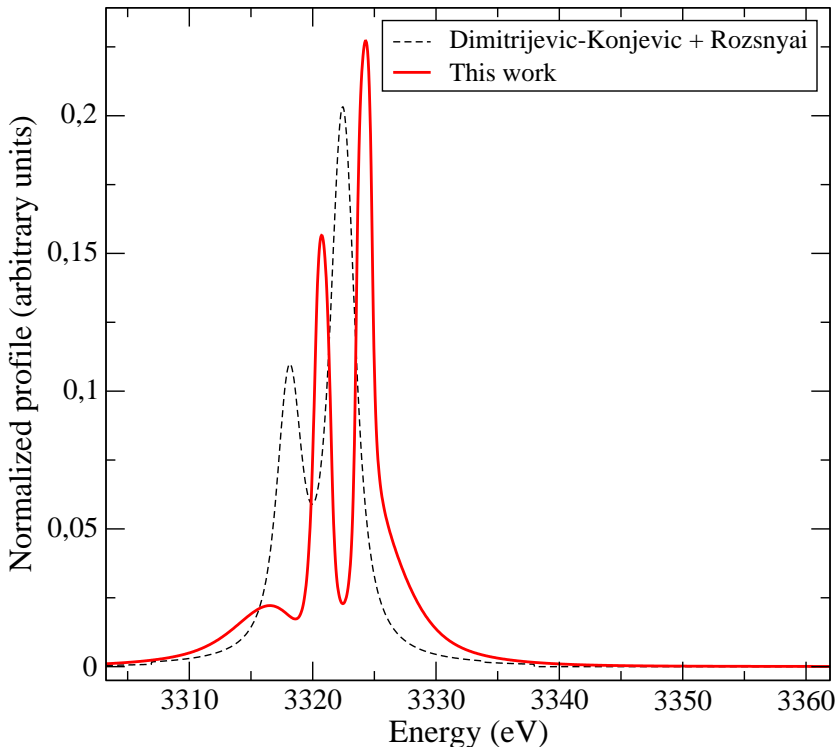


Figure 1: Ly $_{\alpha}$  line for an Ar plasma at  $T_e=T_i=700$  eV and  $\rho=3.98$  g/cm $^3$  (example chosen in Ref. [7]).

is diagonalized in the sub-space of states  $|1s; n\ell m_{\ell}; S\rangle$  with  $S=0$  for singlet states and  $S=1$  for triplet states. For He $_{\alpha}$ , the resonance line ( $1s2p\ ^1P - 1s^2$ ) requires the energies of terms  $1s2s\ ^1S$  and  $1s2p\ ^1P$  and the intercombination line ( $1s2p\ ^3P - 1s^2$ ) the energies of terms  $1s2s\ ^3S$  and  $1s2p\ ^3P$ .

## 4 Interpretation of a “buried-layer” experiment on aluminum

Fig. 3 shows our interpretation of the recently measured emission of aluminum micro-targets buried in plastic (“buried layers”) and heated by an ultra-short laser [10]. Fig. 5 displays the He $_{\beta}$  profile with different models for the microfield distribution function  $W(F)$  (see Fig. 4): Holtmark model, neglecting ionic correlations and electron screening (see Ref. [11] and references therein), Mayer and “nearest neighbour” (NN) distributions, valid for strongly coupled plasmas, and a combination of APEX (Adjustable Parameter EXponential) method with Monte Carlo simulations proposed by Potekhin et al. [11] and parametrized by ionic coupling  $\Gamma = (Z^*e)^2 / (r_{ws}k_B T_i)$  and electron degeneracy  $\kappa = r_{ws} / \lambda_{TF}$  constants,  $r_{ws}$  being the Wigner-Seitz radius and  $\lambda_{TF}$  the Thomas-Fermi screening length. Table 1 shows the values of the full width at half maximum (FWHM) of Ly $_{\alpha,\beta}$  and He $_{\alpha,\beta}$  lines with the new and previous (Refs. [5, 6]) modelings of Stark effect in SCO-RCG.

In the future, we plan to investigate the importance of autoionizing states  $1s2\ell 2\ell'$  and  $1s2\ell 3\ell'$  of He $_{\beta}$  (in the present work we only took into account  $2\ell 2\ell'$ ) and to include the line  $1s3d\ ^1D_2 - 1s^2\ ^1S_0$  induced by the field (mixing states  $1s3d\ ^1D_2$  and  $1s3p\ ^1P_1$ ) as well as the lines  $1s3d\ ^3D_2 - 1s^2\ ^1S_0$  and  $1s3s\ ^3S_1 - 1s^2\ ^1S_0$ . We also started to study the Stark-Zeeman splitting.

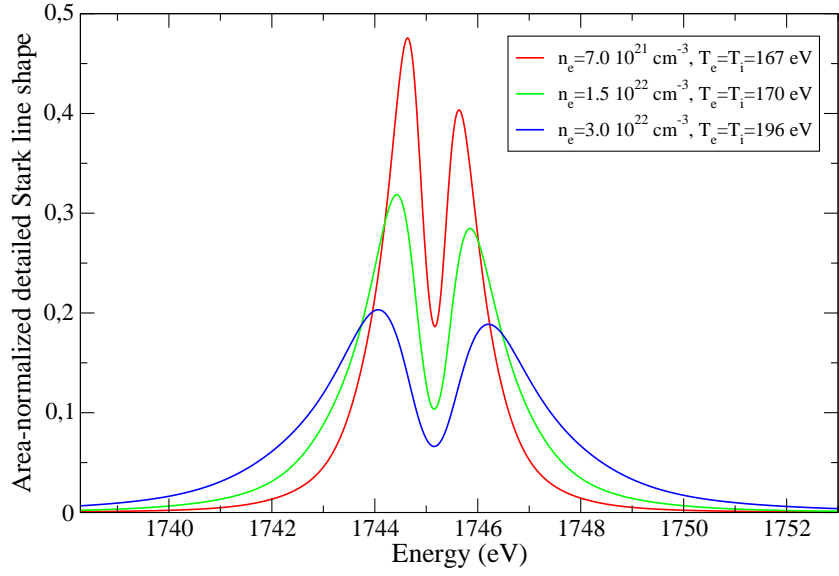


Figure 2:  $Ly_\beta$  line for a Mg plasma in three different conditions (example chosen in Ref. [8]).

Model / FWHM	$Ly_\alpha$	$Ly_\beta$	$He_\alpha$	$He_\beta$
This work	1.80	27.03	2.46	32.84
Dimitrijevic-Konjevic	2.19	53.73	2.07	61.92

Table 1: FWHM of  $Ly_{\alpha,\beta}$  and  $He_{\alpha,\beta}$  lines for an Al plasma at  $T_e=T_i=310$  eV and  $\rho=2.7$  g/cm<sup>3</sup>.

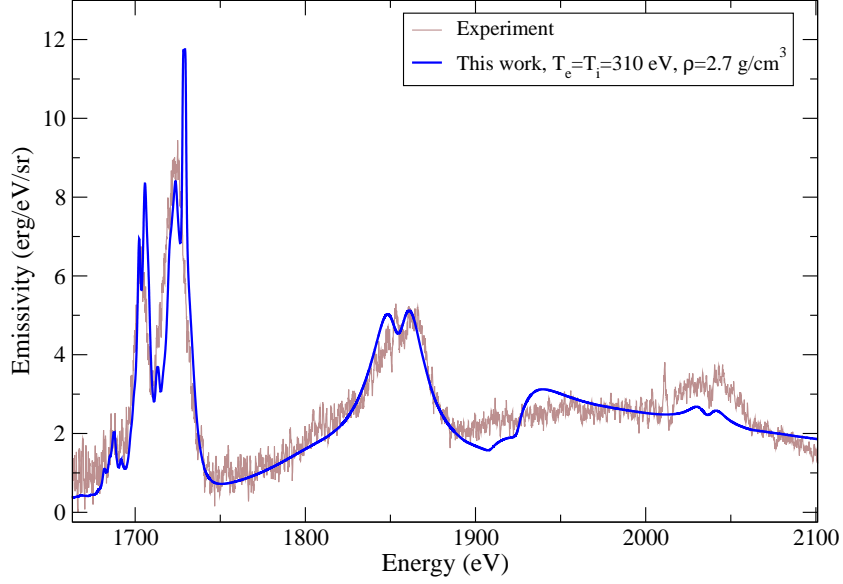


Figure 3: Measured emission of aluminum “buried layers” heated by an ultra-short laser [10] (emissive volume:  $400 \mu\text{m}^2 \times 0.5 \mu\text{m}$ , duration: 3 ps) compared to SCO-RCG prediction.

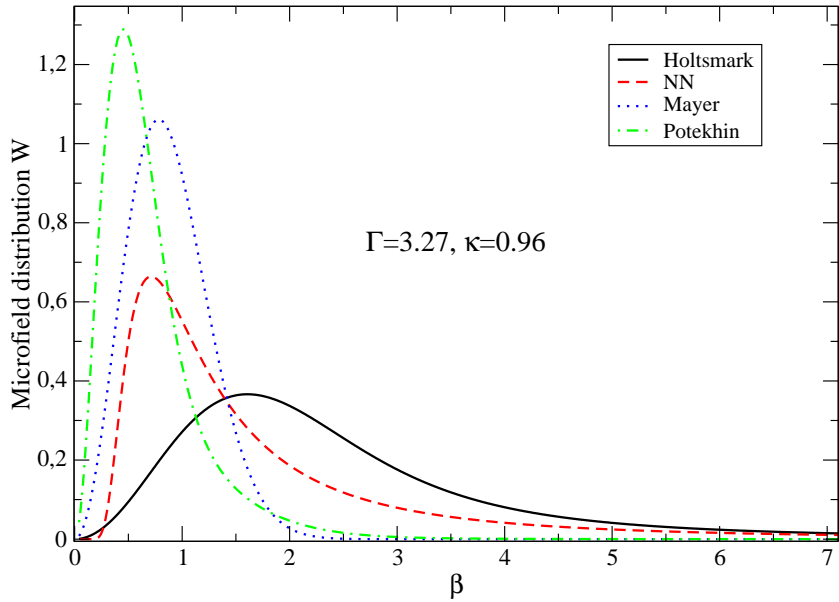


Figure 4: Different microfield distributions for an Al plasma at  $T_e=T_i=310 \text{ eV}$  and  $\rho=2.7 \text{ g/cm}^3$  (units of  $\beta = F/F_0$ , where  $F_0 = Z^*e/r_{ws}^2$ ).

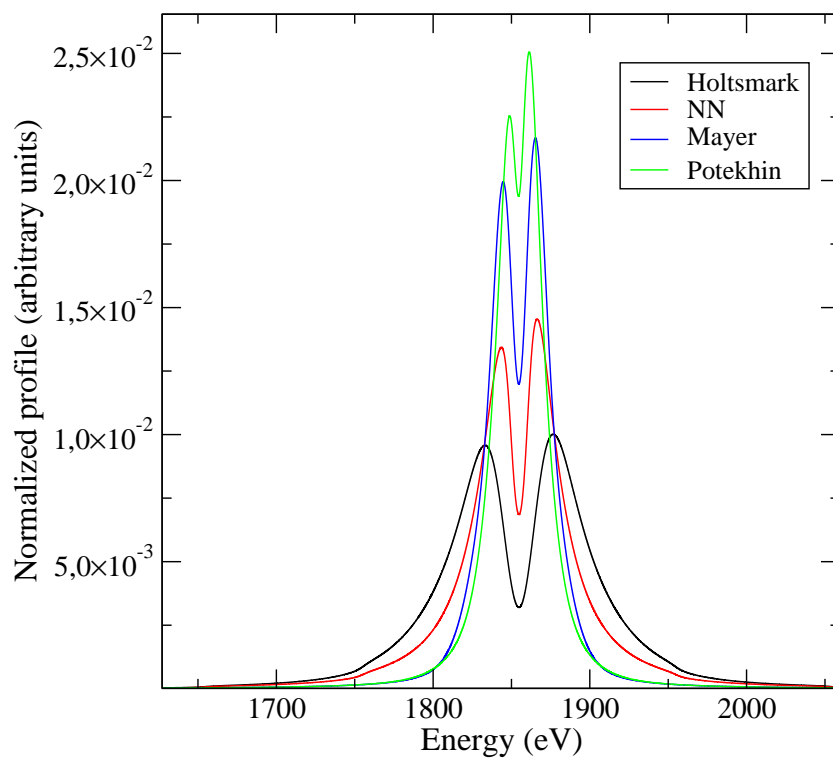


Figure 5: He<sub>β</sub> line for the different microfield distributions of Fig. 4.

## 5 Acknowledgments

We would like to thank V. Dervieux, B. Loupiau and P. Renaudin for providing the experimental spectrum.

## References

- [1] Pain J-C, Gilleron F and Blenski T 2015 *Laser. Part. Beams* **33** 201
- [2] Pain J-C and Gilleron F 2015 *High Energy Density Phys.* **15** 30
- [3] Gilles D and Peyrusse O 1995 *J. Quant. Spectrosc. Radiat. Transfer* **53** 647
- [4] Humlíček J 1979 *J. Quant. Spectrosc. Radiat. Transfer* **21** 309
- [5] Dimitrijević M S and Konjević N 1980 *J. Quant. Spectrosc. Radiat. Transfer* **24** 451
- [6] Rozsnyai B F 1977, *J. Quant. Spectrosc. Radiat. Transfer* **17** 77
- [7] Mancini R C, Iglesias C A, Ferri S, Calisti A and Florido R 2013 *High Energy Density Phys.* **9** 731
- [8] Nagayama T et al. 2014 *Phys. Plasmas* **21** 056502
- [9] Bethe H A and Salpeter E E 1957 *Quantum Mechanics of one- and two- electron atoms* (Berlin: Springer)
- [10] Dervieux V et al. 2015 *High Energy Density Phys.* **16** 12
- [11] Potekhin A Y, Chabrier G and Gilles D 2002, *Phys. Rev. E* **65** 036412